nature microbiology

LETTERS

PUBLISHED: 19 JUNE 2017 | VOLUME: 2 | ARTICLE NUMBER: 17096

Toxoplasma depends on lysosomal consumption of autophagosomes for persistent infection

Manlio Di Cristina[1,2*], Zhicheng Dou[1†], Matteo Lunghi[2], Geetha Kannan[1], My-Hang Huynh[1], Olivia L. McGovern[1], Tracey L. Schultz[1], Aric J. Schultz[1], Alyssa J. Miller[1†], Beth M. Hayes[1†], Wouter van der Linden[3], Carla Emiliani[2], Matthew Bogyo[3], Sébastien Besteiro[4], Isabelle Coppens[5] and Vern B. Carruthers[1*]

Globally, nearly 2 billion people are infected with the intracellular protozoan *Toxoplasma gondii*[1]. This persistent infection can cause severe disease in immunocompromised people and is epidemiologically linked to major mental illnesses[2] and cognitive impairment[3]. There are currently no options for curing this infection. The lack of effective therapeutics is due partly to a poor understanding of the essential pathways that maintain long-term infection. Although it is known that *Toxoplasma* replicates slowly within intracellular cysts demarcated with a cyst wall, precisely how it sustains itself and remodels organelles in this niche is unknown. Here, we identify a key role for proteolysis within the parasite lysosomal organelle (the vacuolar compartment or VAC) in turnover of autophagosomes and persistence during neural infection. We found that disrupting a VAC-localized cysteine protease compromised VAC digestive function and markedly reduced chronic infection. Death of parasites lacking the VAC protease was preceded by accumulation of undigested autophagosomes in the parasite cytoplasm. These findings suggest an unanticipated function for parasite lysosomal degradation in chronic infection, and identify an intrinsic role for autophagy in the *T. gondii* parasite and its close relatives. This work also identifies a key element of *Toxoplasma* persistence and suggests that VAC proteolysis is a prospective target for pharmacological development.

The *Toxoplasma* lysosomal vacuolar compartment (VAC) contains two papain family cysteine proteases termed cathepsin protease L (CPL, toxodb accession no. TGME49_321530) and cathepsin protease B (CPB, TGME49_249670)[4–6]. Upregulated expression of CPL and CPB in chronically infected mice[7] suggests an active role for VAC proteolysis in *Toxoplasma* persistence. To test this prospect, we focused on CPL, because maturation of CPB is dependent on its activity[6], so ablating CPL effectively impairs both proteases. Genetic ablation of CPL in Prugniaud (P) strain parasites, which express cytosolic green fluorescent protein (GFP) during chronic infection[8], was confirmed by PCR, immunofluorescence and immunoblotting (Supplementary Figs 1–3). Consistent with findings in a different strain background[9], PΔ*cpl* acute-stage parasites (tachyzoites) presented a dilated VAC suggestive of organellar dysfunction, a phenotype that was rescued by genetic complementation (Fig. 1a,b). Although CPL-deficient parasites appeared to differentiate normally to chronic-stage bradyzoites within cultured intracellular cysts (Fig. 1c), after differentiation they progressively lost stage-specific expression of GFP (Fig. 1d,e) and viability (Fig. 1f). Re-expression of active CPL restored cyst viability, whereas cysts expressing a catalytically inactive CPL (Fig. 1f) or treated with a CPL inhibitor (morpholinurea-leucyl-homophenyl-vinyl sulfone phenyl, LHVS[9]; Fig. 1g and Supplementary Fig. 4) died. Taken together, these findings suggest a key role for VAC proteolytic activity for maintaining the viability of cultured *Toxoplasma* cysts.

Next, we sought to define the contribution of VAC proteolysis to infection in mice, which are a convenient model and an important natural host for *Toxoplasma gondii*. Consistent with earlier work[10], survival of PΔ*cpl*-infected mice was higher than wild type (WT)-infected mice, indicating a role for CPL in acute virulence (Fig. 2a). Nevertheless, mice infected with 10^6 WT or PΔ*cpl* showed a similar pattern of parasite burden in the first eight days of infection (Fig. 2b)[10], comparable kinetics of parasite entry into the brain (Fig. 2c) and lungs (Supplementary Fig. 5) and similar cytokine profiles (Supplementary Fig. 5). Notably, mice infected with PruΔ*cpl* had substantially fewer cysts, despite comparable kinetics of acute infection (Fig. 2a and Supplementary Fig. 6). Furthermore, although mice infected with the highest dose (10^7) of PΔ*cpl* yielded cysts, these cysts contained markedly enlarged and misshapen bradyzoites (Fig. 2d).

To independently validate these findings we ablated CPL in the highly cystogenic ME49 strain (MΔ*cpl*; Supplementary Fig. 7). Mice infected with MΔ*cpl* produced ~100-fold and ~200-fold fewer cysts than WT-infected mice at 5 weeks and 16 weeks post-infection, respectively. This deficit was partially rescued by re-expressing CPL during the chronic stage, but not when the protease was re-expressed in only the acute stage (Fig. 2e). Overexpression of CPL under the BAG1 chronic-stage-specific promoter might have contributed to incomplete rescue (Supplementary Fig. 7). Finally, WT parasites and strains re-expressing CPL in the chronic stage showed normal brain cyst morphology, whereas the CPL knockout parasite cysts or those with re-expression of CPL only in the acute stage were abnormally granulated and phase dark (Fig. 2f). Collectively, these findings are consistent with a vital role for CPL in persistent neural infection of a mammalian host.

[1]Department of Microbiology and Immunology, University of Michigan Medical School, Ann Arbor, Michigan 48109, USA. [2]Department of Chemistry, Biology and Biotechnology, University of Perugia, Perugia 06122, Italy. [3]Department of Chemical and Systems Biology, Stanford University School of Medicine, Stanford, California 94305, USA. [4]DIMNP-UMR 5235 CNRS, Université de Montpellier, 34095 Montpellier Cedex 5, France. [5]Department of Molecular Microbiology and Immunology, The Johns Hopkins University Bloomberg School of Public Health, Baltimore, Maryland 21205, USA. †Present addresses: Department of Biology, Clemson University, Clemson, South Carolina 29634, USA (Z.D.); Graduate Program in Cellular and Molecular Biology, University of Michigan Medical School, Ann Arbor, Michigan 48109, USA (A.J.M.); Department of Biochemistry and Molecular Biology, University of California at San Francisco, California, 94143 USA (B.M.H.). *e-mail: manlio.dicristina@unipg.it; vcarruth@umich.edu

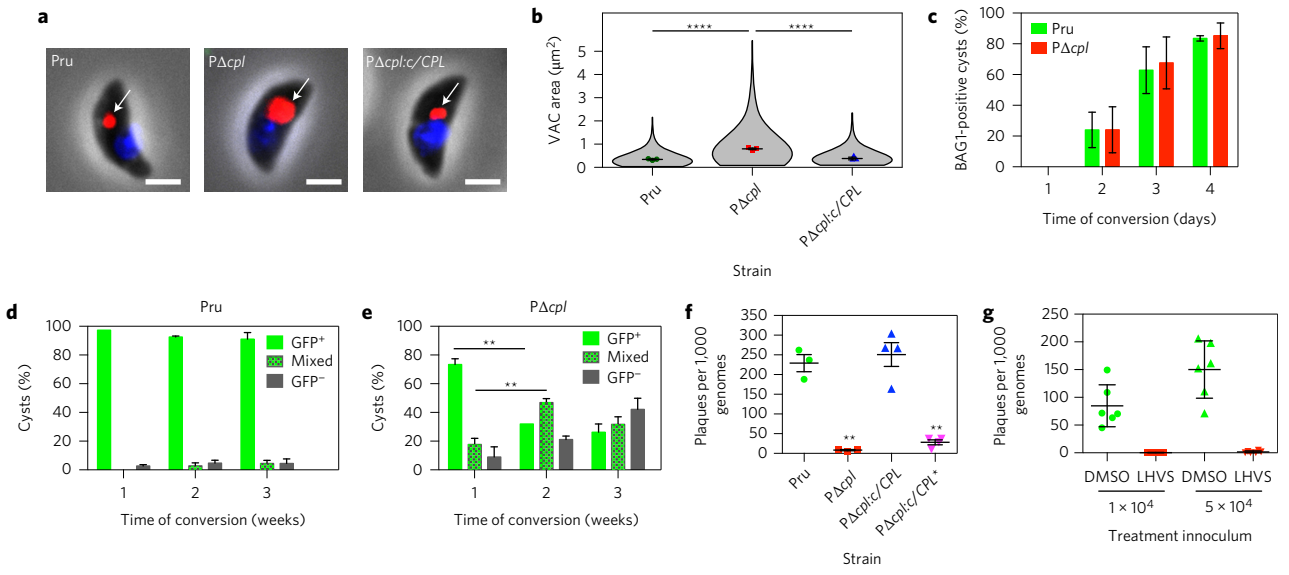

Figure 1 | VAC proteolytic activity is required for *Toxoplasma* viability and persistence *in vitro*. a, Extracellular tachyzoites were stained with anti-CPB (red) to mark the VAC and DAPI (blue) to identify the nucleus. An arrow indicates the localization of the VAC. Scale bars, 2 μm. **b**, Violin plots of VAC size. Data are presented as mean ± s.e.m. of three biological replicates, with the following number of parasites evaluated: Pru, 317, 153, 154; PΔ*cpl*, 271, 177, 176; PΔ*cpl:c/CPL*, 293, 153, 153. Shape indicates the distribution of pooled data. ****$P < 0.0001$, Mann–Whitney test. **c**, *In vitro* differentiation based on expression of the bradyzoite-specific antigen BAG1. Cultures were differentiated for the indicated time, fixed, stained with anti-BAG1, and enumerated by fluorescence microscopy. Bars are presented as mean ± s.e.m. of two biological replicates. Experiment 1 assessed for Pru 205, 214, 204 and 208 parasitophorous vacuoles (PVs) on days 1, 2, 3 and 4, respectively, and for PΔ*cpl*, 209, 211, 213 and 202 PVs, respectively. Experiment 2 assessed for Pru 212, 202, 208 and 202 PVs on days 1, 2, 3 and 4, respectively, and for PΔ*cpl* 205, 207, 214 and 208 PVs, respectively. **d**,**e**, Viability of Pru (**d**) or PΔ*cpl* (**e**) bradyzoites based on stage-specific expression of cytosolic GFP under the LHD2 promoter[8]. Cultures were differentiated and enumerated by fluorescence microscopy. Green bars indicate cysts that are uniformly GFP positive. Checked bars specify cysts that contain GFP-positive and GFP-negative bradyzoites. Grey bars indicate cysts that are uniformly GFP-negative. Data are presented as mean ± s.d. of three biological replicates, each with 100 cysts evaluated. **$P < 0.001$, two-tailed paired Student's *t*-test. **f**, Viability of CPL-proficient and -deficient strains based on plaquing efficiency. Strains were differentiated for 4 weeks, liberated from cysts, quantified by qPCR and inoculated onto fresh cell monolayers for plaque formation. PΔ*cpl:c/CPL** is complemented with catalytically inactive CPL. Bars are presented as mean ± s.e.m. of three (Pru, PΔ*cpl*) or four (PΔ*cpl:c/CPL*, PΔ*cpl:c/CPL**) biological replicates, each with two technical replicates. **$P < 0.01$, Mann–Whitney test. **g**, Viability of Pru bradyzoites differentiated for 1 week before treatment with solvent (DMSO) or 1 μM LHVS for 4 weeks. Viability was measured as in **f**. $n = 2$ biological replicates, each with three technical replicates.

To identify a potential basis for loss of viability, we examined cultured cysts by microscopy and noticed that bradyzoites genetically (PΔ*cpl*) or chemically (LHVS) deficient in CPL activity showed large, dark cytoplasmic inclusions that were absent from WT or complemented parasites (Fig. 3a,b). Stage-specific CPL re-expression during the persistent stage, but not the acute stage, eliminated the inclusions. These findings suggest the aberrant structures result from a lack of CPL expression during the persistent stage and are not a legacy of CPL deficiency during acute-stage infection.

We reasoned that the dark inclusions were due to accumulation of undigested material within the VAC and that some of the material could be derived from autophagy. Autophagy is a process whereby cytoplasmic contents, including organelles, are membrane-encapsulated and degraded within lysosomes[11]. *Toxoplasma* and related apicomplexans, including malaria parasites, express a limited repertoire of autophagy (ATG) proteins[12]. These parasites also unconventionally require certain ATG proteins for maintenance of the apicoplast[13,14], a remnant non-photosynthetic chloroplast. Autophagosome-like structures have been observed under nutrient-limiting conditions[15,16], but the extent to which the parasite encounters such conditions during infection remains unknown. To define the relationship between the intracellular inclusions and autophagosomes, we ectopically expressed a copy of *Toxoplasma* Atg8 fused to the fluorescent protein tdTomato in bradyzoites. WT cysts showed tdTomato-Atg8 fluorescent puncta, suggestive of baseline autophagy during normal parasite encystation (Fig. 3c). However, ablation of CPL or treatment with LHVS augmented tdTomato-Atg8 fluorescence (Fig. 3c), which corresponded to the dark inclusions but not the apicoplast (Supplementary Fig. 8). Mutation of the lipidation site on Atg8 ($Atg8^{G124A}$) in PΔ*cpl* parasites caused diffuse cytosolic fluorescence, indicating that the inclusions are decorated with the lipid-anchored, active form of Atg8 (Fig. 3c). This finding was confirmed by western blotting for Atg8, which showed accumulation of the lipidated Atg8-phosphatidyl serine (Atg8-PE) form in PΔ*cpl* and Pru-LHVS bradyzoites, suggesting an arrest of autophagic flux (Fig. 3d). Taken together, these results imply that autophagosomes develop in WT cysts, but become much more pronounced in the absence of CPL activity. Cysts treated with LHVS developed autophagosomes containing CPL, indicating a defect in the degradation of autophaged material (Fig. 3e). In some cases, CPL occupied a rim around the autophagosome, suggesting recent fusion of the autophagosome and VAC (Fig. 3e). Transmission electron microscopy revealed electron-dense inclusions in LHVS-treated Pru bradyzoites that appeared to contain undigested material, including putative organellar remnants (Fig. 3f).

Similar to the Pru strain, autophagosome accumulation in ME49 bradyzoites was strictly dependent on the absence of CPL expression (Supplementary Fig. 9). ME49 CPL-deficient bradyzoites also displayed remnants of organelles including endoplasmic reticulum (ER) within autophagosomes (Fig. 4a), which showed a time-dependent increase in size following differentiation (Fig. 4b). WT ME49 bradyzoites presented similar VAC intraluminal structures that were more prominent in day 7 bradyzoites, suggesting active turnover of autophagic structures after differentiation. Whereas WT

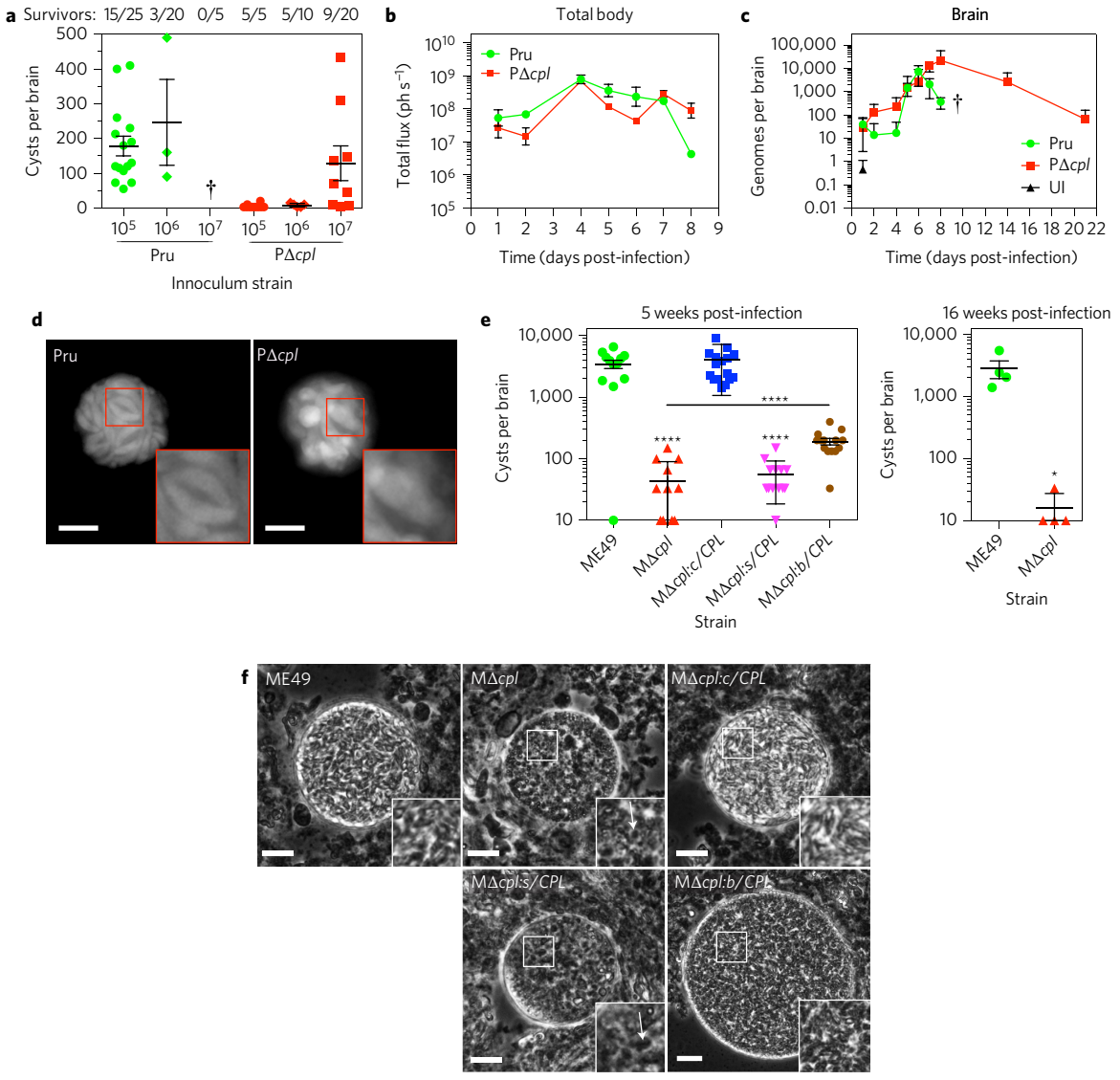

Figure 2 | VAC proteolytic function is required for *Toxoplasma* persistence in infected mice. a, Burden of brain cysts in Pru- and PΔ*cpl*-infected C57BL/6 mice. Mice were infected with the indicated inoculum for 4 weeks, humanely euthanized, and cysts were enumerated microscopically in brain homogenates. Each data point indicates cyst burden in one mouse. Data are presented as mean ± s.e.m. of data pooled as follows: Pru 10^5, four experiments; Pru 10^6, three experiments; Pru 10^7, one experiment; PΔ*cpl* 10^5, one experiment; PΔ*cpl* 10^6, one experiment; PΔ*cpl* 10^7, three experiments. All mice in the Pru 10^7 group succumbed to infection during the acute stage, as indicated by a dagger. The number of mice that survived 4 weeks is indicated, as well as the total number of mice in each group. **b**, Parasite burden throughout the body of infected mice. C57BL/6 mice (four per group) were infected i.p. with 10^6 tachyzoites. Total body parasite burden was determined by bioluminescence imaging and measurement of light flux (photons per second, ph s^{-1}) from parasites expressing firefly luciferase. Data are presented as mean ± s.e.m. from one experiment. **c**, Mice were infected as in **b**, and parasite burden in the brain was measured by qPCR. Data are presented as mean ± s.e.m. from one experiment. A dagger indicates that Pru-infected mice succumbed to infection before imaging on day 10. UI, uninfected. **d**, Live fluorescence microscopy of cysts in brain homogenates. Brain homogenates were prepared 4 weeks post-infection for fluorescence microscopy of cytosolic GFP in cysts. Insets: enlargements of boxed regions including two Pru bradyzoites and one PΔ*cpl* bradyzoite. Scale bars, 10 μm. **e**, Burden of brain cysts in mice infected with ME49 WT or transgenic strains. Female CBA/J mice (20 mice per group) were infected i.p. with 500 tachyzoites and humanely euthanized for cyst enumeration 5 weeks (left) or 16 weeks (right) post-infection. Five-week post-infection data are pooled from two experiments. Sixteen-week post-infection data are from one experiment. MΔ*cpl:c/CPL* is complemented with CPL under its cognate promoter, MΔ*cpl:s/CPL* is complemented with CPL under the SAG1 promoter for expression only in tachyzoites, MΔ*cpl:b/CPL* is complemented with CPL under the BAG1 promoter for expression only in bradyzoites. Data are presented as mean ± s.e.m. $^*P < 0.05$, $^{****}P < 0.0001$, Mann–Whitney test comparing MΔ*cpl* to ME49, MΔ*cpl:s/CPL* to ME49, or MΔ*cpl:b/CPL* to MΔ*cpl* (line). **f**, Phase-contrast microscopy of ME49 WT or transgenic strain cysts in brain homogenates. Arrows indicate granular structures in CPL-deficient cysts. Scale bars, 10 μm.

ME49 cysts appeared healthy on both day 4 and day 7, some day 7 MΔ*cpl* cysts contained degenerate bradyzoites with compromised integrity (Supplementary Fig. 10), consistent with a critical function for CPL in bradyzoite viability.

In summary, we have shown that VAC proteolytic function is required for *Toxoplasma* persistence in culture and in infected mice. We also find that blocking CPL activity causes accumulation of material, including organellar remnants in the VAC before cyst death, indicating a key role for turnover of autophagosomes during *Toxoplasma* persistence. Whereas previous studies of autophagy in *T. gondii* depended upon induction via drug treatment or starvation conditions[15,16], our work suggests an

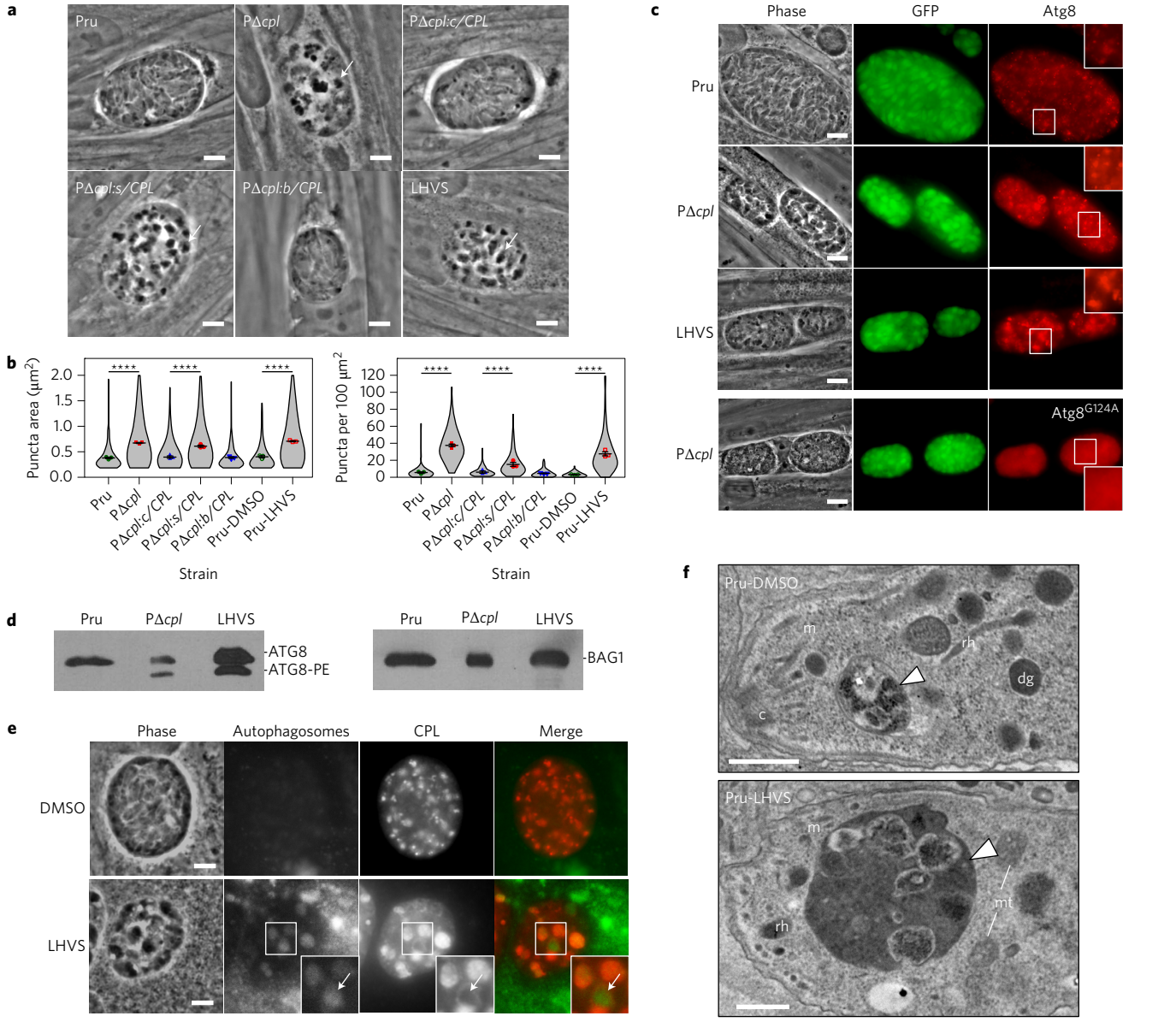

Figure 3 | CPL-deficient bradyzoites develop Atg8-positive autophagosomes associated with the VAC. a, Phase-contrast microscopy of *in vitro* encysted bradyzoites differentiated for 7 days. Arrows indicate cytoplasmic inclusions in CPL-deficient strains. Scale bars, 5 μm. **b**, Quantification of dark inclusion size (area of individual puncta, left) and number (per 100 μm^2 of cyst area, right) shown as violin plots. Data are presented as mean ± s.e.m. of three biological replicates. The following number of total cysts/puncta, respectively, were quantified: Pru 74/409; PΔ*cpl* 102/3,812; PΔ*cpl:c/CPL* 120/743; PΔ*cpl:s/CPL* 86/1,324; PΔ*cpl:b/CPL* 101/464; Pru-DMSO 75/237 and Pru-LHVS 110/3,024. Shape indicates distribution of the pooled data. ****$P < 0.0001$, Mann–Whitney test. **c**, Fluorescence microscopy of autophagosomes in bradyzoites expressing tdTomato-Atg8. Bradyzoites were differentiated for 7 days, fixed and viewed for bradyzoite-specific expression of GFP and tdTomato-Atg8. Examples in the top three rows are of parasites expressing WT tdTomato-Atg8, whereas the bottom row shows parasites expressing a tdTomato-Atg8 bearing a glycine to alanine mutation rendering it refractory to lipidation. Scale bars, 10 μm. The same scale applies to the fluorescence images, which were captured and processed identically. **d**, Western blots of bradyzoite lysates probed with anti-Atg8 or anti-BAG1. **e**, Fluorescence microscopy of autophagosomes in Pru bradyzoites treated with solvent (DMSO) or 1 μM LHVS. Bradyzoites were differentiated for 7 days, treated for 4 days, stained for autophagosomes with cytoID (green), fixed and stained with anti-CPL (red). An arrow indicates an example of CPL at the periphery of an autophagosome shown as an inset of the boxed area. Scale bars, 5 μm. The same scale applies to the fluorescence images. **f**, Transmission electron microscopy of bradyzoites differentiated for 1 week. c, conoid; m, microneme; rh, rhoptry; dg, dense granule; mt, mitochondrion. Arrows indicate putative VACs. Scale bars, 500 nm.

intrinsic role for autophagy in bradyzoites without specific treatment. Autophagy following encystation could be required to renew organelles for the chronic stage or it might reflect a stringent response if the cyst wall physically limits resource acquisition from the host. Although the cyst wall is permeable to LHVS, this inhibitor does not cross the blood–brain barrier[17]. Priority will be given to identifying central nervous system penetrant inhibitors of CPL to potentially abate *Toxoplasma* persistence.

Methods

Host cells and parasite cultures. Human foreskin fibroblasts (HFFs) were not specifically authenticated, but the cultures were derived from low-pass cryostocks (ATCC CRL-1634) every three months and maintained in Dulbecco's modified Eagle medium (DMEM Gibco) containing 10% fetal bovine serum (D10 media). *T. gondii* strains PruΔ*ku80*, ME49 and their mutants were propagated *in vitro* by serial passage on monolayers of HFFs[18]. *In vitro* tachyzoite-to-bradyzoite conversion was induced by exposing parasite cultures to pH 8.2, as described previously[19]. LHVS treatment of parasites was performed by daily replacement of media

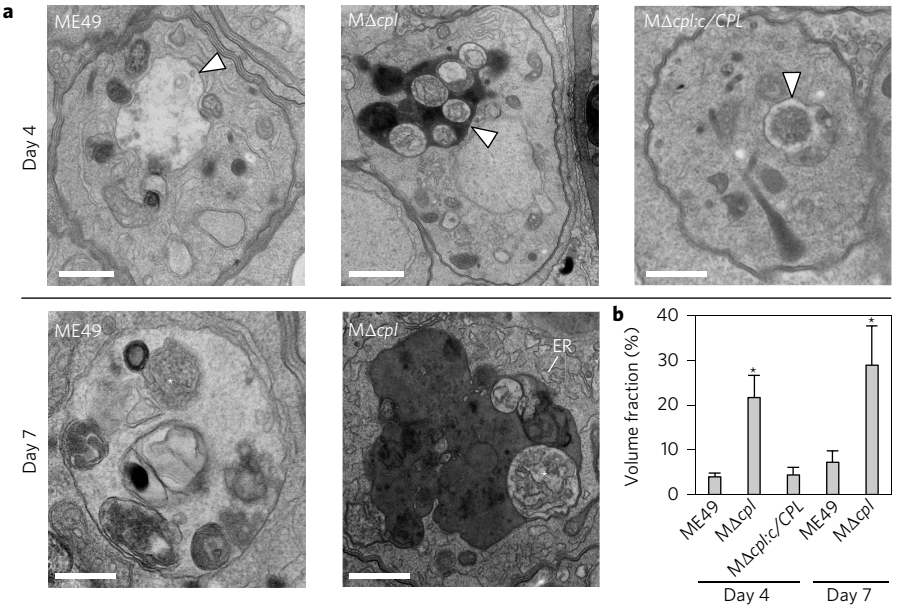

Figure 4 | CPL-deficient bradyzoites develop undigested autophagosomes containing organellar remnants. a, Electron microscopy of intracellular ME49, MΔ*cpl* and MΔ*cpl*:CPL comparing the morphology of VAC (arrows) at day 4, showing electron density for this compartment in MΔ*cpl* bradyzoites. High-magnification views at day 7 reveal cytosolic material (asterisks) resembling piecemeal of the cytoplasm (ME49) and ER (MΔ*cpl*), suggestive of autophagy activities occurring in the VAC with delayed degradation in the mutant reflected by electron-dense luminal content. Scale bars, 500 nm. **b**, Volume fraction of VAC from representative electron micrographs of parasitophorous vacuoles (PVs) from each group (29 and 25 PVs for ME49 at day 4 and 7, respectively; 30 and 32 PVs of MΔ*cpl* at day 4 and 7, respectively and 25 PVs for MΔ*cpl*:CPL at day 4) showing significant increase of this compartment in parasites lacking CPL compared to control strains. Volume fraction equals the area of the organelle divided by the area of the cell multiplied by 100. Bars indicate mean ± s.d. $^*P < 0.005$, unpaired Student's *t*-test.

containing 1 μM LHVS diluted from a 1 mM stock in DMSO. HFF cells and parasite strains were routinely tested for mycoplasma contamination.

Generation of transgenic *T. gondii* strains. PruΔ*ku80LUC* (hereafter Pru) and PruΔ*ku80LUC*Δ*cpl* (PΔ*cpl*) strains used to generate additional transformants in this study are based on PruΔ*ku80* (ref. 8) and have been described previously[10]. CPL complement strains PΔ*cpl:c/CPL* and PΔ*cpl:c/CPL** (catalytically inactive C31A mutant) were generated using vectors described in ref. 6 modified by replacing the chloramphenicol acetyltransferase (CAT) cDNA with that encoding bleomycin resistance (BLE). To target the complementation plasmids to the Ku80 locus by single cross-over homologous recombination, we cloned into *Bam*HI and *Sac*I restriction sites 3′ to BLE a 1,664 bp PCR fragment encompassing nucleotide sequence 2753961–2752298 of ME49 chromosome XI (primers ku80 Fw1/ku80 Rv1). These vectors were linearized with *Nde*I in the middle of the Ku80 fragment, and integrated into the PruΔ*cpl* strain, as shown in Supplementary Fig. 1b. Stage-specific complement strains PΔ*cpl:s/CPL* and PΔ*cpl:b/CPL* were created by replacing the *CPL* promoter in the *CPL* complement vector with that of *SAG1* (sequence from −1185 to −1) or *BAG1* (sequence from −1232 to −1) for expression exclusively in tachyzoites or bradyzoites, respectively[20]. SAG1/CPL and BAG1/CPL vectors were linearized with *Xba*I or *Bcl*I, respectively, for non-disruptive single-crossover integration into the *SAG1* or *BAG1* locus of PruΔ*cpl*, as shown in Supplementary Fig. 1c,d.

ME49Δ*cpl* (hereafter MΔ*cpl*) was created using a CRISPR/Cas9 double-cut strategy described by Long and colleagues[21] where the first gRNA sequence (gRNA1) was targeted close to the CPL initiation codon and the second gRNA (gRNA2) near the stop codon, as shown in Supplementary Fig. 7a. Co-transfection of ME49 with this sgRNA CRISPR/Cas9 plasmid (40 μg) and a PCR amplicon consisting of *BLE* flanked by CPL-homology arms (~3,000 bp; 10 μg) successfully resulted in *cpl* deletion. MΔ*cpl:c/CPL*, MΔ*cpl:s/CPL* and MΔ*cpl:b/CPL* complement strains were generated by random integration of the same vectors used for the Pru strains, except that *BLE* was replaced with a dihydrofolate reductase (*DHFR*) cDNA conferring resistance to pyrimethamine.

Pru strains expressing tdTomato-ATG8 or a tdTomato-ATG8^{G124A} lipidation mutant were generated by modifying the pTub-tdTomato-TgATG8-CAT plasmid described in Leveque *et al.*[13] via replacement of *CAT* with *BLE* and cloning in a larger tubulin promoter fragment encompassing −2730 to −1 relative to the tubulin start codon. Plasmids were linearized with *Nar*I at −1318 for single-crossover integration into the tubulin locus. The tdTomato-ATG8 expression cassette was also introduced into ME49 and MΔ*cpl* strains by random integration and chloramphenicol selection.

T. gondii transfections were performed as described previously by Lunghi and co-workers[22]. Correct integration was identified by PCR analysis of single clones using the Phire Tissue Direct PCR Master Kit (ThermoFisher Scientific).

Immunoblotting and immunofluorescence. Immunoblotting and immunofluorescence were performed as described previously[23,24]. For immunoblotting, mouse anti-CPL (ref. 9) and rabbit anti-actin[25] antibodies were diluted 1:5,000 and 1:10,000, respectively. For immunofluorescence, rabbit anti-CPL and mouse anti-CPB (ref. 6) were diluted 1:500 and 1:250, respectively. Autophagosomes were stained using a cytoID Autophagy Detection Kit 2.0 (Enzo) according to the manufacturer's instructions.

Analysis of VAC size. Syringe-released tachyzoites were allowed to invade HFF cells for 2 h at 37 °C followed by washing with PBS. Newly invaded parasites were again syringe-released and affixed to slides coated with Cell-Tak (Corning), fixed with 4% paraformaldehyde and stained with mouse anti-CPB to identify the VAC. Images were acquired by focusing on the VAC signal in the maximum number of parasites within a field of view and captured on a Zeiss Axiovert Observer Z1 inverted fluorescence microscope equipped with a ×100 oil objective and an AxioCAM MRm camera and processed using Zeiss Axiovision 4.3 software. For Pru, PΔ*cpl*, PΔ*cpl:c/CPL* and PΔ*cpl:c/CPL* strains, VAC size was measured with Zeiss Axiovision 4.3 software by defining the area of anti-CPB immunofluorescence. VAC measurements were only performed on VACs that were within focus. Equal parameters for the capture and enumeration of images were consistently applied to all samples. We cannot rule out that fixation differentially affected VAC size for the different strains assessed in the study.

Bradyzoite conversion, viability and analysis of dark inclusions. Bradyzoite conversion was assessed by counting vacuoles. Vacuoles displaying more than 50% of parasites stained by the rabbit anti-BAG1 antibodies were considered positive. HFF monolayers grown onto coverslips were infected with mechanically extruded tachyzoites for 16 h, and then the media were replaced with alkaline media to induce bradyzoite conversion. At least 200 parasite vacuoles were counted in two independent experiments for each time point.

Loss of bradyzoite viability was measured by counting GFP-positive versus GFP-negative cysts at different time points of conversion. Samples were blinded. Infected HFF monolayers were cultivated in alkaline media for 1, 2 or 3 weeks and then fixed in 4% paraformaldehyde for 20 min; at least 100 cysts were assessed for GFP positivity under a fluorescence microscope.

The viability of bradyzoites was assessed by combining plaque assay and quantitative polymerase chain reaction (qPCR) analysis of genome number. *In vitro* cysts were generated by maintaining infected HFF in alkaline media in six-well plates. After selected times, infected monolayers were washed three times with HBSS, and cysts contained in one well were mechanically extruded from the HFFs by syringing several times through 26G needles. Released cysts were centrifuged at 1,500*g* for 10 min at room temperature and resuspended in 500 μl HBSS. Then, 500 μl of pre-warmed 2× pepsin solution (0.026% pepsin in 170 mM NaCl and 60 mM HCl,

final concentration) was added and the sample was incubated for 30 min at 37 °C. Reactions were stopped by adding 94 mM Na_2CO_3, removing the supernatant after centrifugation at 1,500*g* for 10 min at room temperature and resuspending pepsin-treated parasites in 1 ml of DMEM without serum. After calculating number of parasites per ml, 100 or 500 parasites per well were added to six-well plates containing confluent monolayers of HFFs in D10 media. Parasites were grown undisturbed for 12 days and plaque assays were performed by ethanol fixation for 2 min, staining with 0.2% crystal violet for 5 min and followed by several washes with double-distilled H_2O. Images of the wells were scanned, and plaque number and size were analysed with ImageJ. Seven hundred microlitres of the initial 1 ml of pepsin-treated parasites was used for gDNA purification using the DNeasy Blood & Tissue Kit (Qiagen). Genomic DNA was eluted in a final volume of 100 µl, and 8 µl was analysed by qPCR using tubulin primers TUB2.RT.F and TUB2.RT.R to determine the number of parasite genomes per microlitre. qPCR analyses were performed using Brilliant II SYBR Green QPCR Master Mix (Agilent) and a Stratagene Mx3000PQ-PCR machine.

To quantify dark inclusions in bradyzoites, images of *in vitro* differentiated cysts were taken using a Zeiss Axio inverted microscope equipped with an Axiocam MRM charge-coupled device (CCD) camera using a ×100 oil objective. ImageJ software was used to identify cysts by Max Entropy thresholding on the GFP channel followed by selection of objects with areas between 130 and 1,900 µm^2. Particles (puncta) under the GFP mask were further analysed by automatic local thresholding on the phase image using the Phansalkar method, with the following parameters: radius = 5 µm; *k* value = 0.5; *r* value = 0.5. Dark inclusions (puncta) were measured from the resulting binary mask by particle analysis according to the following: size = 0.18–2.00 µm; circularity = 0.50–1.00. These parameters were chosen based on accuracy in a head-to-head comparison against manual counting. A total of 10,013 puncta were analysed from 668 cysts.

Assessment of Atg8 lipidation. Parasites grown in HFF cells were converted to bradyzoites in alkaline medium for 5 days and treated with 1 µM LHVS in conversion medium for an additional 2 days. Bradyzoites were isolated by scraping and syringing infected monolayers several times through a 26G needle and subsequent pepsin treatment for 30 min at 37 °C to release bradyzoites and selectively kill tachyzoites. Parasite pellets were solubilized in SDS sample buffer, and lysates corresponding to 3×10^6 parasites per lane were separated in 15% SDS–PAGE gels containing 6 M urea, transferred to polyvinylidene fluoride (PVDF) membranes and incubated with affinity-purified rabbit anti-TgATG8 (diluted 1:500, provided by William Sullivan Jr). Blots were then incubated with an anti-rabbit HRP antibody, and immunoreactive bands were visualized with the West Pico Chemiluminescent Substrate (Thermo Scientific) and exposure to film. Blots were then stripped and reprobed with rabbit anti-BAG1 (1:5,000)[26] as a loading control and to assess bradyzoite conversion.

Electron microscopy of *in vitro* cysts. HFF monolayers grown in six-well plates were infected with 5×10^4 tachyzoites in D10 media. After 16 h, the D10 medium was replaced with alkaline media (pH 8.2) to induce bradyzoite conversion. *In vitro* cysts were processed for electron microscopy (EM) analysis 4 or 7 days post bradyzoite conversion. EM preparation of samples was carried out by washing the infected monolayers with cold PBS three times, followed by fixation with 2.5% glutaraldehyde (EMS, catalogue no. 16210) in 0.1 M sodium cacodylate buffer (pH 7.4) for 1 h at room temperature. After fixation, infected cells were gently scraped to detach large sheets, centrifuged at 1,500*g* for 10 min and washed three times with 0.1 M sodium cacodylate (pH 7.4) buffer and stored in the same buffer at 4 °C until processed for EM as described in ref. 27 before examination with a Philips CM120 electron microscope under 80 kV. Quantitative morphometric analyses of VAC from 25 to 32 representative electron micrographs from each group (ME49, MΔ*cpl* and MΔ*cpl:CPL*) were performed at low magnification to ensure the entire parasite fit into the field of view and could be analysed as described in ref. 28 by using the standard formula for randomly orientated cell and structures.

Competition assay with LHVS. Brains containing ME49 cysts were collected from infected mice and homogenized in 1 ml of 1× PBS by sequential syringing through 19G and 23G needles. Homogenized brain material was then incubated for 30 min with either 200 nM BODIPY-LHVS (BO-LHVS) alone or a 1:1 or 1:10 mixture of BO-LHVS and LHVS. After three washes with 1× PBS, brain material was fixed with 4% paraformaldehyde and stained with rabbit anti-CPL antibodies at a 1:200 dilution followed by Alexa 594-conjugated goat anti-rabbit antibodies. Stained brain material was then allowed to adhere to slides coated with Cell-Tak adhesive (Corning). Images were captured with a Zeiss Axiovert Observer Z1 inverted fluorescence microscope and an AxioCAM MRm camera and processed using Zeiss Axiovision 4.3 software.

Mouse studies. Seven-week-old female C57BL/6 mice (Charles River) were randomly assigned to groups and infected intraperitoneally (i.p.) with 10^5, 10^6 or 10^7 tachyzoites of WT or transgenic PruΔ*ku80* strains (type II genotype). Group sizes and numbers of experiments are as follows: Pru 10^5, 25 mice total, four experiments; Pru 10^6, 20 mice total, three experiments; Pru 10^7, 5 mice total, one experiment; PΔ*cpl* 10^5, 10 mice total, one experiment; PΔ*cpl* 10^6, 5 mice per group, one experiment; PΔ*cpl* 10^7, 20 mice total, three experiments. Mice were humanely euthanized 4 weeks post-infection. Assessing the statistical differences in cyst burden between mice infected with Pru and PruΔ*cpl* was complicated by the absence of cyst data from the mice that did not survive infection. Because mice that die from the infection often have higher burden and become moribund and must be euthanized before the 4 weeks when cysts are counted, enumeration of cysts from those that survive probably underestimates differences. Accordingly, statistical analysis was not provided. WT or genetically manipulated ME49 strains were injected with 500 tachyzoites i.p. in seven-week-old female CBA/J mice (Jackson Laboratory). Data were pooled from two experiments, with 13 mice per group in experiment 1, and 7 mice per group in experiment 2. Mice infected with ME49 strains were euthanized humanely at 5 or 16 weeks post-infection. The mouse brains were placed in 1 ml sterile PBS and individually minced with scissors, vortexed and homogenized by three or four passages through a 22G needle and syringe. Two 100 µl brain samples (200 µl total) from mice infected with PruΔ*ku80* strains were placed on a glass microscope slide and then mounted on a coverslip. Cysts were enumerated without knowledge of the samples' treatment group under an inverted fluorescence phase-contrast microscope by exploiting fluorescence emitted by GFP expressed under the control of the bradyzoite-specific LDH2 promoter[3]. Three 10 µl samples (30 µl total) of brain homogenates from mice infected with ME49 strains were instead analysed by phase-contrast microscopy to enumerate cysts. Sample sizes were chosen based on previous studies. Mice were randomly assigned to groups and samples were blinded for enumeration of cysts. Animal studies described here adhere to a protocol approved by the Committee on the Use and Care of Animals of the University of Michigan.

Bioluminescence imaging. Seven-week-old female albino C57B/6 mice (four per strain, based on investigator experience) were i.p. injected with 10^6 Pru or 4×10^6 PΔ*cpl* parasites, which constituted equal inoculation of infectious parasites based on plaque assays. Bioluminescence was assessed as described in ref. 10. Briefly, images were taken at 1, 2, 4, 5, 6, 7 and 8 days post-infection using a Xenogen IVIS 200 system 10 min after i.p. injected with 200 µl of 40 mg ml^{-1} D-luciferin in PBS. Mice were anaesthetized with inhaled isoflurane during imaging. The intensities of bioluminescence signals were quantified using LiveImage software coupled with the Xenogen IVIS 200. All four mice in both groups were alive for imaging on day 6, and three mice in both groups were imaged on day 7. One Pru-infected mouse and three PΔ*cpl*-infected mice were imaged on day 8 when the experiment was terminated.

Quantitative PCR. Brains of infected and uninfected control mice were dissected, weighed, and immediately stored at −20 °C. Tissue was then thawed, and 25 mg of tissue per sample was homogenized with a pestle in 1× PBS and then passaged four to five times through a 22G needle. Genomic DNA was extracted using a Qiagen DNeasy Blood and Tissue Kit. To create a standard curve, known numbers of cultured tachyzoites were spiked into 25 mg of homogenized brain tissue from age-matched uninfected mice at concentrations of 10^{-1}, 10^0, 10^1, 10^2, 10^3, 10^4 and 10^5 tachyzoites per milligram of brain tissue. Fifty nanograms of DNA from each sample were used to run quantitative real-time PCR using primers against a *Toxoplasma*-specific 529 bp repeat element[29] (Tox-9 Forward, 5′ AGGAGAGATATCAGGACTGTAG, Tox-11 Reverse 5′ GCGTCGTCTCGTCT AGATCG). Treated and control sample threshold cycle (CT) values were compared against the standard curve to extrapolate the number of *Toxoplasma* genomes per brain. All samples were run in biological and technical triplicates. Samples with a CT value at or above 40 were considered to have undetectable amplification and were set to zero *Toxoplasma* genomes per brain.

Cytokine analysis. Seven-week-old female C57B/6 mice injected with 10^6 Pru or 4×10^6 PΔ*cpl* parasites were euthanized by CO_2 fixation at 1, 2, 4, 5, 6, 7, 8, 14 and 21 days post-infection. Uninfected controls were euthanized at 1, 6, 14 and 21 days post-infection to be used as baseline controls. Blood was collected by cardiac puncture, and serum was separated by centrifugation. Levels of cytokines (interferon-γ, interleukin-10 and tumour-necrosis factor-α) were assessed by capture enzyme-linked immunosorbent assay. Data were analysed and plotted in GraphPad Prism 6.

Data availability. All relevant data are included in the paper or the Supplementary Information.

Received 7 December 2016; accepted 11 May 2017; published 19 June 2017

References

1. Montoya, J. G. & Liesenfeld, O. Toxoplasmosis. *Lancet* **363,** 1965–1976 (2004).
2. Sutterland, A. L. *et al.* Beyond the association. *Toxoplasma gondii* in schizophrenia, bipolar disorder, and addiction: systematic review and meta-analysis. *Acta Psychiatr. Scand.* **132,** 161–179 (2015).
3. Bharti, A. R. *et al.* Latent toxoplasma infection and higher *Toxoplasma gondii* immunoglobulin G levels are associated with worse neurocognitive functioning in HIV-infected adults. *Clin. Infect. Dis.* **63,** 1655–1660 (2016).

4. Parussini, F., Coppens, I., Shah, P. P., Diamond, S. L. & Carruthers, V. B. Cathepsin L occupies a vacuolar compartment and is a protein maturase within the endo/exocytic system of *Toxoplasma gondii*. *Mol. Microbiol.* **76,** 1340–1357 (2010).
5. Miranda, K. *et al.* Characterization of a novel organelle in *Toxoplasma gondii* with similar composition and function to the plant vacuole. *Mol. Microbiol.* **76,** 1358–1375 (2010).
6. Dou, Z., Coppens, I. & Carruthers, V. B. Non-canonical maturation of two papain-family proteases in *Toxoplasma gondii*. *J. Biol. Chem.* **288,** 3523–3534 (2013).
7. Pittman, K. J., Aliota, M. T. & Knoll, L. J. Dual transcriptional profiling of mice and *Toxoplasma gondii* during acute and chronic infection. *BMC Genomics* **15,** 806 (2014).
8. Fox, B. A. *et al.* Type II *Toxoplasma gondii* KU80 knockout strains enable functional analysis of genes required for cyst development and latent infection. *Eukaryot. Cell* **10,** 1193–1206 (2011).
9. Dou, Z., McGovern, O., Di Cristina, M. & Carruthers, V. *Toxoplasma gondii* ingests and digests host cytosolic proteins. *mBio* **5,** e01188–14 (2014).
10. Larson, E. T. *et al. Toxoplasma gondii* cathepsin L is the primary target of the invasion-inhibitory compound morpholinurea-leucyl-homophenyl-vinyl sulfone phenyl. *J. Biol. Chem.* **284,** 26839–26850 (2009).
11. Parzych, K. R. & Klionsky, D. J. An overview of autophagy: morphology, mechanism, and regulation. *Antioxid. Redox Signal.* **20,** 460–473 (2014).
12. Besteiro, S. Which roles for autophagy in *Toxoplasma gondii* and related apicomplexan parasites? *Mol. Biochem. Parasitol.* **184,** 1–8 (2012).
13. Leveque, M. F. *et al.* Autophagy-related protein ATG8 has a noncanonical function for apicoplast inheritance in *Toxoplasma gondii*. *mBio* **6,** e01446–15 (2015).
14. Tomlins, A. M. *et al. Plasmodium falciparum* ATG8 implicated in both autophagy and apicoplast formation. *Autophagy* **9,** 1540–1552 (2013).
15. Besteiro, S., Brooks, C. F., Striepen, B. & Dubremetz, J. F. Autophagy protein Atg3 is essential for maintaining mitochondrial integrity and for normal intracellular development of *Toxoplasma gondii* tachyzoites. *PLoS Pathog.* **7,** e1002416 (2011).
16. Ghosh, D., Walton, J. L., Roepe, P. D. & Sinai, A. P. Autophagy is a cell death mechanism in *Toxoplasma gondii*. *Cell. Microbiol.* **14,** 589–607 (2012).
17. Barclay, J. *et al.* Role of the cysteine protease cathepsin S in neuropathic hyperalgesia. *Pain* **130,** 225–234 (2007).
18. Di Cristina, M. *et al.* Transformed *Toxoplasma gondii* tachyzoites expressing the circumsporozoite protein of *Plasmodium knowlesi* elicit a specific immune response in rhesus monkeys. *Infect. Immun.* **67,** 1677–1682 (1999).
19. Galizi, R. *et al.* Evidence of tRNA cleavage in apicomplexan parasites: half-tRNAs as new potential regulatory molecules of *Toxoplasma gondii* and *Plasmodium berghei*. *Mol. Biochem. Parasitol.* **188,** 99–108 (2013).
20. Di Cristina, M. *et al.* Temporal and spatial distribution of *Toxoplasma gondii* differentiation into bradyzoites and tissue cyst formation *in vivo*. *Infect. Immun.* **76,** 3491–3501 (2008).
21. Long, S., Wang, Q. & Sibley, L. D. Analysis of noncanonical calcium-dependent protein kinases in *Toxoplasma gondii* by targeted gene deletion using CRISPR/Cas9. *Infect. Immun.* **84,** 1262–1273 (2016).
22. Lunghi, M., Galizi, R., Magini, A., Carruthers, V. B. & Di Cristina, M. Expression of the glycolytic enzymes enolase and lactate dehydrogenase during the early phase of *Toxoplasma* differentiation is regulated by an intron retention mechanism. *Mol. Microbiol.* **96,** 1159–1175 (2015).
23. Di Cristina, M., Spaccapelo, R., Soldati, D., Bistoni, F. & Crisanti, A. Two conserved amino acid motifs mediate protein targeting to the micronemes of the apicomplexan parasite *Toxoplasma gondii*. *Mol. Cell Biol.* **20,** 7332–7341 (2000).
24. Spano, F. *et al.* The SAG5 locus of *Toxoplasma gondii* encodes three novel proteins belonging to the SAG1 family of surface antigens. *Int. J. Parasitol.* **32,** 121–131 (2002).
25. Dobrowolski, J. M. & Sibley, L. D. *Toxoplasma* invasion of mammalian cells is powered by the actin cytoskeleton of the parasite. *Cell* **84,** 933–939 (1996).
26. Zhang, Y. W. *et al.* Disruption of the *Toxoplasma gondii* bradyzoite-specific gene BAG1 decreases *in vivo* cyst formation. *Mol. Microbiol.* **31,** 691–701 (1999).
27. Coppens, I. & Joiner, K. A. Host but not parasite cholesterol controls *Toxoplasma* cell entry by modulating organelle discharge. *Mol. Biol. Cell* **14,** 3804–3820 (2003).
28. Opperdoes, F. R. *et al.* Purification, morphometric analysis, and characterization of the glycosomes (microbodies) of the protozoan hemoflagellate *Trypanosoma brucei*. *J. Cell Biol.* **98,** 1178–1184 (1984).
29. Reischl, U., Bretagne, S., Kruger, D., Ernault, P. & Costa, J. M. Comparison of two DNA targets for the diagnosis of toxoplasmosis by real-time PCR using fluorescence resonance energy transfer hybridization probes. *BMC Infect. Dis.* **3,** 7 (2003).

Acknowledgements

This work was supported by National Institutes of Health grants R01AI120627 (to V.B.C. and M.D.C.), R01GM111703 (to M.B.) and R01AI060767 (to I.C.). Z.D. and A.J.S. received fellowship support from the American Heart Association. B.M.H. and G.K. were supported by National Institutes of Health training grant T32AI007528. O.L.M. was supported by a National Institutes of Health Ruth Kirschstein National Research Service Award F31AI118274. The authors thank S. Meshinchi and J. Whitfield at the University of Michigan for help with electron microscopy and cytokine analysis, respectively, as well as the Johns Hopkins University Microscopy facility. The authors thank L. Weiss, W. Sullivan Jr and L.D. Sibley for the provision of antibodies for this study.

Author contributions

M.D.C., Z.D., M.L., O.L.M., G.K., M.-H.H., A.J.M., B.M.H., C.E. and V.B.C. designed the experiments. M.D.C., A.J.S., A.J.M., B.M.H. and V.B.C. wrote the manuscript. W.v.d.L. performed chemical synthesis. M.D.C., Z.D., M.L., O.L.M., G.K., M.H.-H., T.L.S., A.J.S., A.J.M., B.M.H. and I.C. performed the experiments. C.E., M.B. and S.B. provided advice or reagents that were essential for completion of the study. All authors discussed the findings and commented on the manuscript.

Additional information

Supplementary information is available for this paper.

Reprints and permissions information is available at www.nature.com/reprints.

Correspondence and requests for materials should be addressed to M.D.C. and V.B.C.

How to cite this article: Di Cristina, M. *et al. Toxoplasma* depends on lysosomal consumption of autophagosomes for persistent infection. *Nat. Microbiol.* **2,** 17096 (2017).

Publisher's note: Springer Nature remains neutral with regard to jurisdictional claims in published maps and institutional affiliations.

Competing interests

The authors declare no competing financial interests.